Bureau of Mines Report of Investigations/1986

Effect of Alloying Elements on Oxidation of Low-Chromium Alloys

By Je M. Oh

UNITED STATES DEPARTMENT OF THE INTERIOR

Report of Investigations 9047

Effect of Alloying Elements on Oxidation of Low-Chromium Alloys

By Je M. Oh

UNITED STATES DEPARTMENT OF THE INTERIOR
Donald Paul Hodel, Secretary

BUREAU OF MINES
Robert C. Horton, Director

Library of Congress Cataloging in Publication Data:

Oh, Je M. (Je Myung)
Effect of alloying elements on oxidation of low-chromium alloys.

(Report of investigations; 9047)

Bibliography: p. 12.

Supt. of Docs. no.: I 28.23:9047.

1. Chrome-nickel steel. 2. Oxidation. 3. Steel alloys. I. Title. II. Series: Report of investigations (United States. Bureau of Mines); 9047.

TN23.U43 [TN799.C5] 622 s [620.1'723] 86-600219

CONTENTS

ILLUSTRATIONS

TABLES

UNIT OF MEASURE ABBREVIATIONS USED IN THIS REPORT

°C	degree Celsius	min	minute
cm/s	centimeter per second	mm	millimeter
g	gram	µm	micrometer
h	hour	µm/min	micrometer per minute
in	inch	pct	percent
kV	kilovolt	wt pct	weight percent
mg/cm^2	milligram per square centimeter		

EFFECT OF ALLOYING ELEMENTS ON OXIDATION OF LOW-CHROMIUM ALLOYS

By Je M. Oh[1]

ABSTRACT

The Bureau of Mines is conducting research to determine the high-temperature oxidation resistance of substitute stainless steels (SS) containing two less strategic elements, Al and Si, instead of Cr. Chromium is considered to be a critical and strategic metal.

Although the Cr content was reduced to 8 wt pct, the alloys showed better oxidation resistance than did 304 SS containing 18 wt pct Cr. Specifically, the alloys that contained Fe-8Cr-16Ni with combinations of Al and Si showed excellent oxidation resistance even at temperatures up to 1,000° C.

In this study, the effects of the alloying elements on oxidation kinetics and morphology of oxides were investigated using a Cahn Rg electrobalance, scanning electron microscopy, an energy-dispersive X-ray analyzer, X-ray diffraction, and an electron microprobe. Aluminum and silicon additions in combinatin were more effective in providing oxidation resistance than either element was alone.

INTRODUCTION

One Bureau of Mines research goal is to minimize the requirements for domestically scarce minerals through substitution and conservation. Chromium, the element that impacts the characteristics of oxidation and corrosion resistance to stainless steels by forming a protective chromium oxide scale, is considered to be a particularly vulnerable strategic metal because the United States has no commercial Cr deposits. Therefore, there is interest in investigating low-Cr alloys that could substitute for stainless steels in some applications.

For an alloy to have oxidation properties similar to those of stainless steels, it should contain at least one element whose oxide is stable, protective, and adherent to the base metal. Aluminum and silicon are the two most common, inexpensive elements, besides Cr, whose oxides have these characteristics. Most of the alloys being considered as possible stainless substitutes contain at least one of these elements. Nine alloys were developed by the Bureau of Mines and tested at different temperatures and times for systematic evaluation; their compositions are shown in table 1. To stabilize the austenite microstructure, large amounts of Ni were added. Although the United States has no commercial Ni deposits, such deposits exist in Canada.

[1]Metallurgist, Albany Research Center, Bureau of Mines, Albany, OR.

TABLE 1. - Alloy composition,[1] weight percent

Alloy	Cr	Ni	Si	Al	Alloy	Cr	Ni	Si	Al
A.....	0	16	0	0	F.....	8.06	15.91	3.25	0.93
B.....	8	0	0	0	G.....	8	16.01	1.27	2.8
C.....	8	16	0	0	H.....	7.93	16	0	2.84
D.....	7.94	15.9	3.25	0	I.....	7.98	16	3.37	2.87
E.....	7.96	15.85	0	.95					

[1]Balance Fe.

ACKNOWLEDGMENT

The author wishes to thank Stanley Rhoads, chemist, Albany Research Center, for his help in constructing the TGA system and valuable discussion during this work.

MATERIALS AND EXPERIMENTAL PROCEDURES

Alloys were prepared from electrolytic grades of Fe, Cr, Ni, high-purity Al, and ferrosilicon. These materials were vacuum-arc-melted into 50-g buttons in a helium atmosphere. The furnace was evacuated and purged with helium twice before being placed under final vacuum. The buttons were hot-rolled to 2-mm sheets at 1,050° C with 20-pct reduction of thickness in each pass. After being cut, the specimens were descaled and polished down to 600 grit on both sides to remove the scale formed during hot rolling. They were then ultrasonically cleaned in soap solution, and degreased with alcohol, followed by acetone. The 304 SS was obtained commercially and tested for comparison purposes.

A Cahn Rg electrobalance[2] was used to obtain kinetic data (fig. 1). In the Cahn Rg electrobalance method, the specimen is suspended from the servo loop, and the displacement caused by weight change is measured and recorded continuously. Continuous recording is the main advantage of the Cahn Rg electrobalance. A Sartorius electronic analytical balance also was used for recording weight change of specimens periodically removed from the furnace. The furnace was mounted on a vertical track so that it could be preheated to a reaction temperature without affecting the specimen. The preheated furnace was raised to the position where the specimen was centered in the constant-temperature zone. The specimen temperature was monitored using a thermocouple near the specimen. To reduce preoxidation during preheating; the specimen was heated to the desired reaction temperature in <5 min in argon. When the specimen reached the reaction

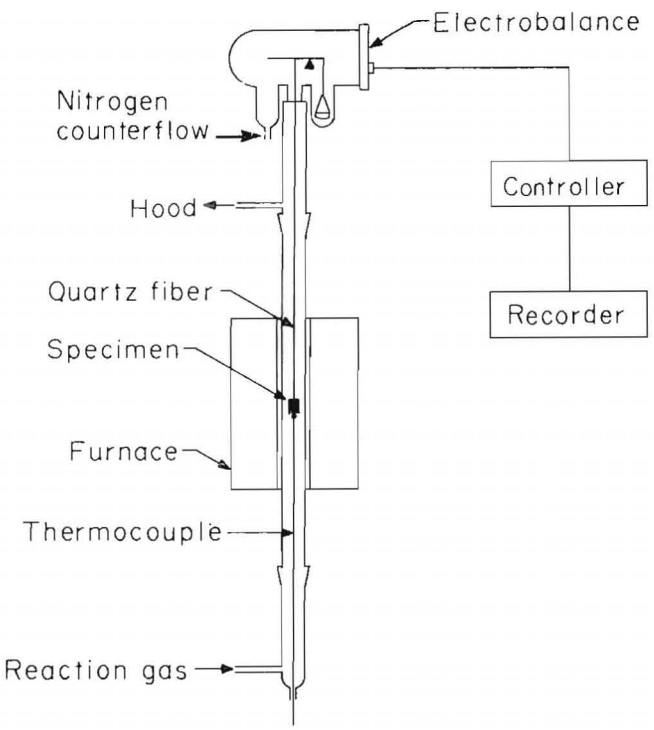

FIGURE 1.—Schematic diagram of electrobalance assembly.

[2]Reference to a specific product or manufacturer does not constitute endorsement by the Bureau of Mines.

temperature, dry air was purged into reaction tube at the linear rate of 1 cm/s. The air was dried with H_2SO_4 and Drierite.

Experimental times and temperatures ranged from 20 to 1,000 h and from 600° to 1,000° C. Thermal cycling also was employed to determine thermal shock resistance of the oxide. The oxidized specimens were examined using scanning elctron microscopy (SEM), an energy-dispersive X-ray analyzer (EDXA), X-ray diffraction, optical microscopy, and an electron microprobe. Some specimens were mounted in epoxy and cross-sectioned to obtain elemental profiles.

RESULTS

Oxidation of the experimental alloys was investigated at 600°, 750°, 900°, and 1,000° C for 20 to 1,000 h in dry air. The experimental results are presented in two sections: (1) thermogravimetric data and (2) morphology and composition of oxide scale and base metal.

THERMOGRAVIMETRIC DATA

At 600° C, alloys D, F, G, H, and I were oxidized for up to 1,000 h. The five alloy specimens were oxidized for 500 h. At the end of that time, the specimens were removed from the furnace, weighed, and then replaced in the furnace for an additional 500 h. The weight change was measured with a Sartorius electronic analytical balance that has an accuracy of ±0.1 mg. The data are summarized in table 2. The average surface area of the specimens was about 12 cm^2. All alloys had extremely small weight gains. Alloy D showed the most weight gain, while alloys G and I showed the least.

Figure 2 illustrates the thermogravimetric data for several alloys at 750° C; 304 SS was tested and the data included for comparison. Since alloys C and E have higher oxidation rates, they are plotted on a different scale. Alloy E, which contained 0.95 wt pct Al, oxidized slightly less than alloy C, which had no Al. Alloy H contained 2.84 wt pct Al and exhibited good oxidation resistance. Alloys F, G, and I, containing both Al and Si, showed excellent oxidation resistance. Alloys F and I showed the same reaction rate, so alloy I was not included.

TABLE 2. - Weight change versus time at 600° C, milligram per square centimeter

Alloy	After 500 h	After 1,000 h
D	0.04	0.06
F	.02	.03
G	.01	.02
H	.02	.03
I	.01	.02

Figure 3 presents the thermogravimetric results of nine alloys tested at 900° C with thermal cycling. Again, 304 SS was included for comparison purposes. Almost identical reaction kinetics are shown for alloys C and E in figure 3*A*, indicating that a small addition of Al had no effect on the kinetics at this temperature. The oxidation rates of alloys A and B were reduced after thermal cycling. However, the oxidation rates of alloys C and E were not affected by thermal cycling. Breakaway oxidation was observed in alloy H during thermal cycling (fig. 3*B*). As

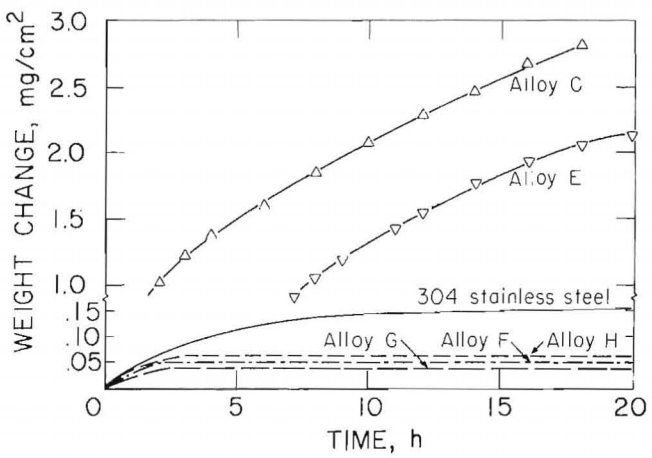

FIGURE 2.—Reaction kinetics of several alloys for 20 h of oxidation at 750° C.

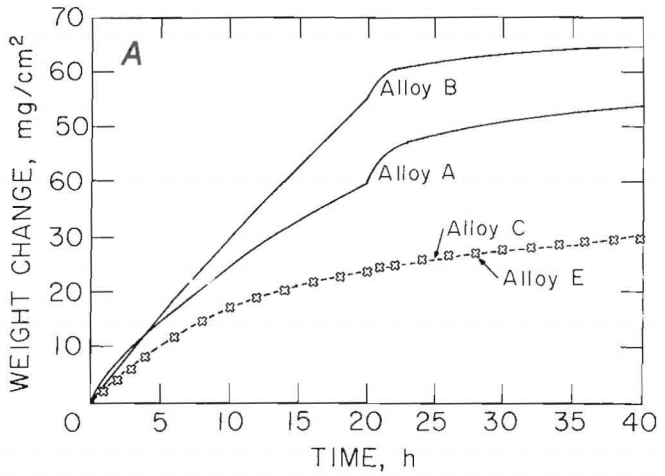

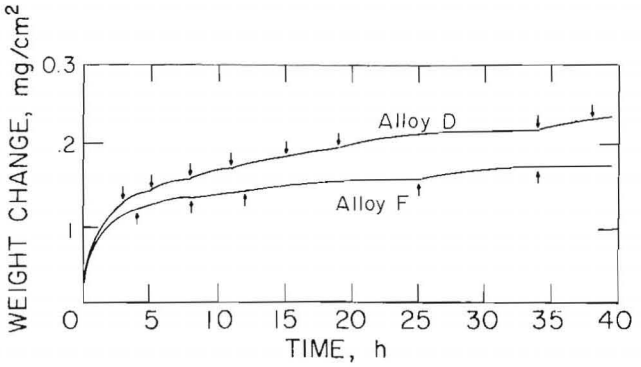

FIGURE 4.—Reaction kinetics of alloys D and F with several thermal cyclings at 900° C. Each arrow indicates end of a thermal cycle with continuous plotting of the weight change.

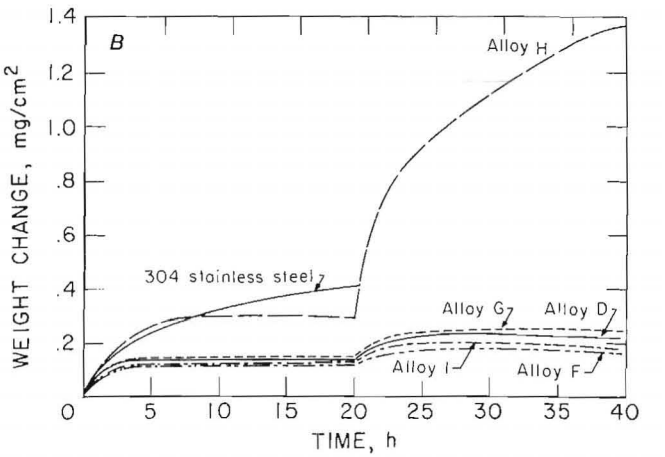

FIGURE 3.—Reaction kinetics of alloys A-I and 304 stainless steel with single thermal cycling.

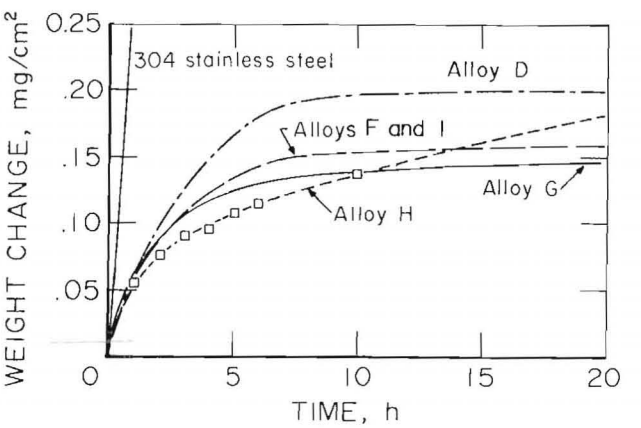

FIGURE 5.—Reaction kinetics of several alloys at 1,000° C.

shown in figure 3*B*, alloys D, F, G, and I have better oxidation resistance than does 304 SS. At 900° C, additions of Al and Si to the alloys produced different results. Alloy D, which contained 3.25 wt pct Si, exhibited good oxidation and thermal shock resistance, while alloy H, which contained 2.84 wt pct Al, exhibited breakaway oxidation.

Alloys D and F were chosen for evaluation of thermal shock resistance at 900° C. These results are plotted in figure 4. During each cycle, the specimen was removed from the furnace and cooled to room temperature before being replaced in the furnace. Both alloys have good thermal shock resistance. Alloy F gained slightly less weight than did alloy D.

Alloys D, F, G, H, and I were oxidized at 1,000° C to obtain further information on oxidation kinetics. Figure 5 shows that all these alloys, except H, have good oxidation resistance at 1,000° C. The dramatic weight gain of 304 SS at 1,000° C shows why the alloy is not normally used at this temperature. Alloy H underwent paralinear-type oxidation kinetics; this alloy had an unacceptably high oxidation rate when thermally cycled (fig. 6). Again, alloys F and G exhibited good thermal shock resistance. The third thermal cycle of alloy H was carried out at 900° C.

MORPHOLOGY AND COMPOSITION OF OXIDE SCALE AND BASE METAL

The morphology and composition of the oxide scale and base metal were examined by optical microscopy, SEM, EDXA, X-ray diffraction, and electron microprobe.

The oxide scales that formed at 600° and 750° C were so thin they were difficult to analyze. As shown in figure 7, no visible oxide was formed after 1,000 h of oxidation at 600° C for alloy F. At 750° C, the oxide was so thin after 1,000 h of oxidation that it did not even cover the polishing grooves (fig. 8).

Alloys A, B, C, and E formed thick oxides at 900° C. Figure 9 illustrates the typical columnar growth of these oxide scales formed on alloy A. The oxide was intentionally broken to show the columnar grain structures. Figure 10 illustrates the nodules formed on alloy C after 40 h of oxidation. X-ray diffraction analysis of alloy C indicated that the oxide was mainly Fe_2O_3 with a minor trace of Fe- and Ni-containing spinel.

The morphology of the oxide was totally changed when Si was added. Figure 11 shows the morphology of the oxide formed on alloy D. The very thin oxide was spalled as a fine powder during cooling. EDXA spot analyses were conducted at points *1* (top of oxide) and *2* (below the oxide), as noted in figure 11. The ZAF[3] correction was used to obtain a better

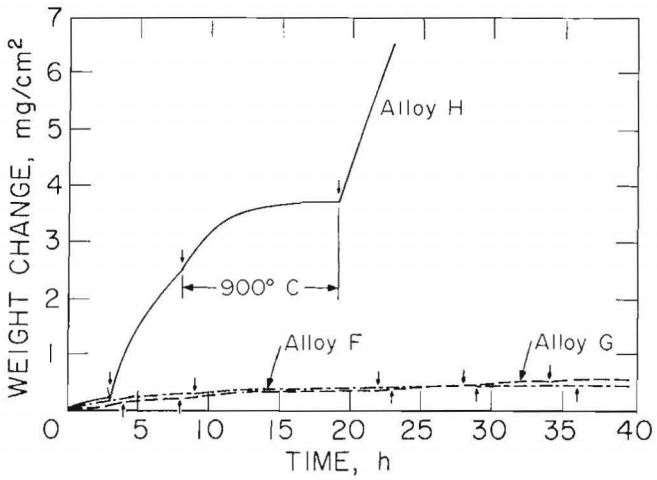

FIGURE 6.—Effect of thermal cycling on oxidation kinetics of alloys at 1,000 °C.

[3]Z=atomic number effect; A=absorption effect; F=fluorescence effect.

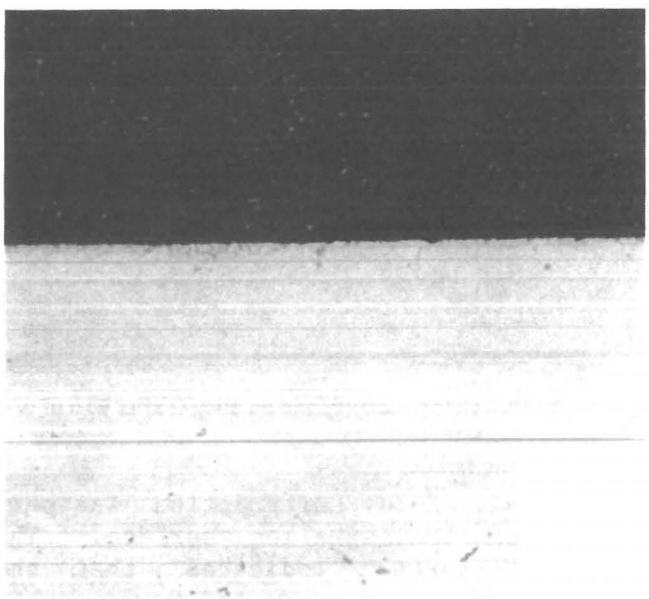

FIGURE 7.—Cross-sectional view of alloy F after 1,000 h of oxidation at 600 ° C (X 400).

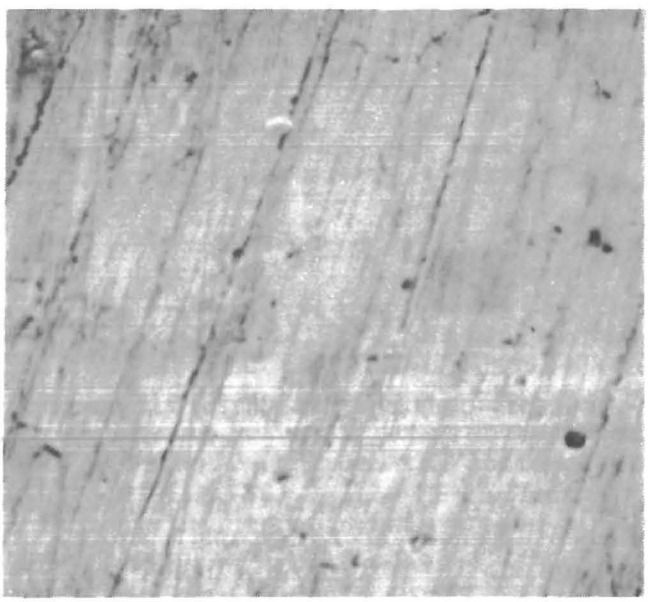

FIGURE 8.—SEM photomicrograph of surface of alloy F after 1,000 h of oxidation at 750 ° C (X 2,000).

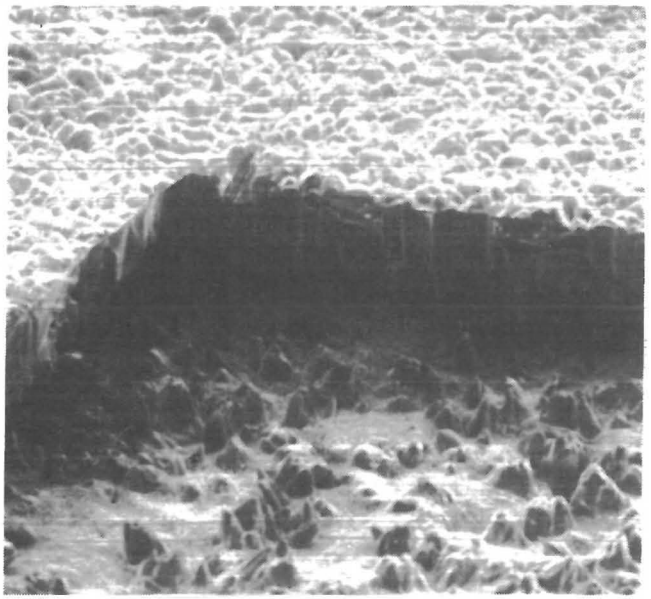

FIGURE 9.—Columnar oxide scale formed on alloy A after 40 h of oxidation at 900° C (X 210).

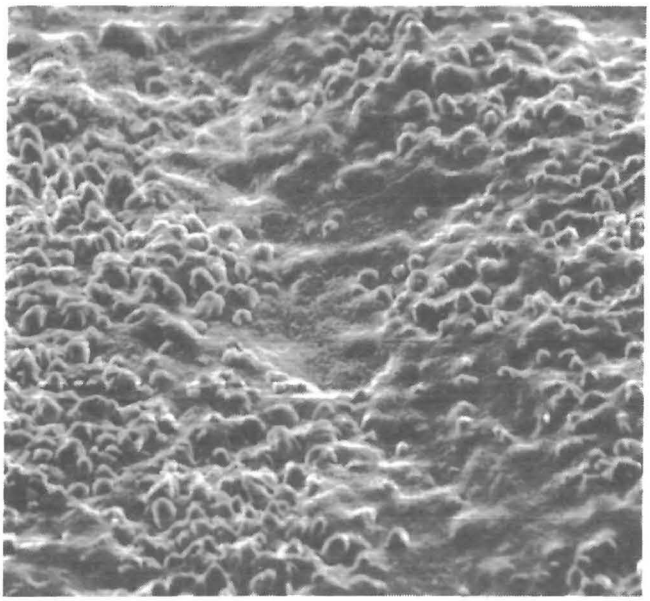

FIGURE 10.—Oxide nodules formed on alloy C after 40 h of oxidation at 900° C (X 500).

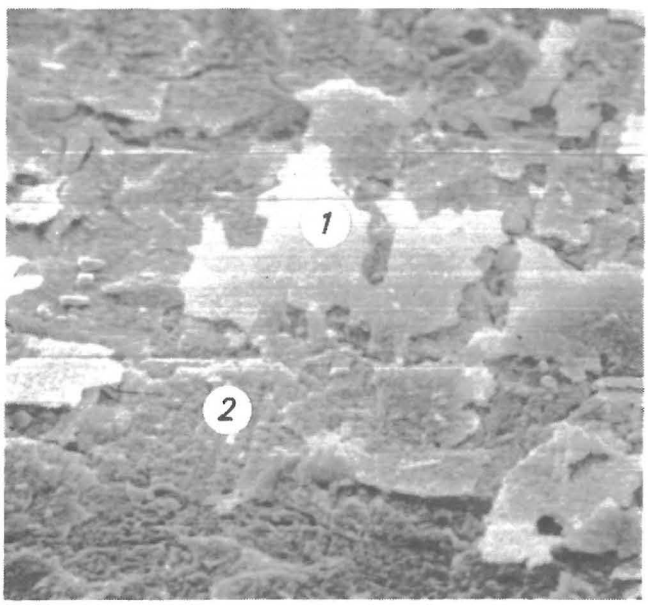

FIGURE 11.—Oxide scale formed on alloy D after 40 h of oxidation at 900° C (X 700).

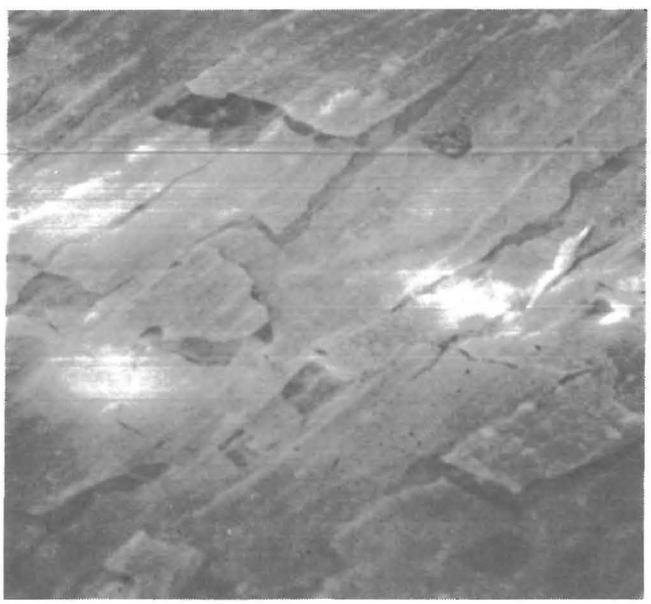

FIGURE 12.—Oxide scale formed on alloy G after 40 h of oxidation at 900° C (X 2,000).

quantitative analysis. The quantitative elemental analyses for areas *1* and *2* are presented in table 3. These analyses show that Cr is the main element in the oxide on alloy D. Since the oxide was not thick enough to separate from the base metal, X-ray diffraction was performed on the specimen surface. The X-ray diffraction indicates that the existing phases are γ-Fe and Cr_2O_3.

When Al is added, the oxide scales appear to be more adherent to the base

TABLE 3. - Quantitative EDXA elemental analyses

Alloy	Conditions		Element, wt pct				
	Temp, °C	Time, h	Al	Cr	Fe	Ni	Si
D	1,000	20	ND	75.3	18.4	3.1	2.2
D, area 1[1]	900	40	ND	98.8	16.2	2.5	2.1
D, area 2[1]	900	40	ND	5	94.8	16.5	2.5
G	1,000	20	39.6	45.5	8.4	5.9	2.9
G	900	40	89.41	9.2	2.3	.2	.89

ND Not detected. [1]See figure 11 for areas 1 and 2 of alloy D.

metal. Alloy G shows better scale adherence than does alloy D (fig. 12). As presented in table 3, Al is a main element in the oxide at 900° C. Alloy H, which previously exhibited breakaway oxidation after thermal cycling, has formed nodules (fig. 13).

At 1,000° C, the morphology of the oxide and base metal has a more distinctive appearance than at 900° C. Figures 14 and 15 illustrate the surface morphologies of alloys D and G after oxidation for 20 h at 1,000° C without thermal cycling. Alloy D has many spalled areas, and alloy G has convoluted oxide morphology. High Cr was observed in the scale of alloy D, while EDXA indicated that both Al and Cr were the main elements in alloy G, as reported in table 3. Figure 16 shows the cross-sectional view and EDXA X-ray maps of alloy F, which was thermally cycled several times during 40 h of oxidation. The scale is mainly Cr-rich; regions of internal oxidation are present in the base metal substrate (fig. 16*C*). No concentration gradients of Si were observed at the metal-scale interface. The alloy G specimen, which also had been thermally cycled several times during 40 h of oxidation, had more regions of internal oxidation, as well as deeper internal oxide penetration, than were observed for alloy F.

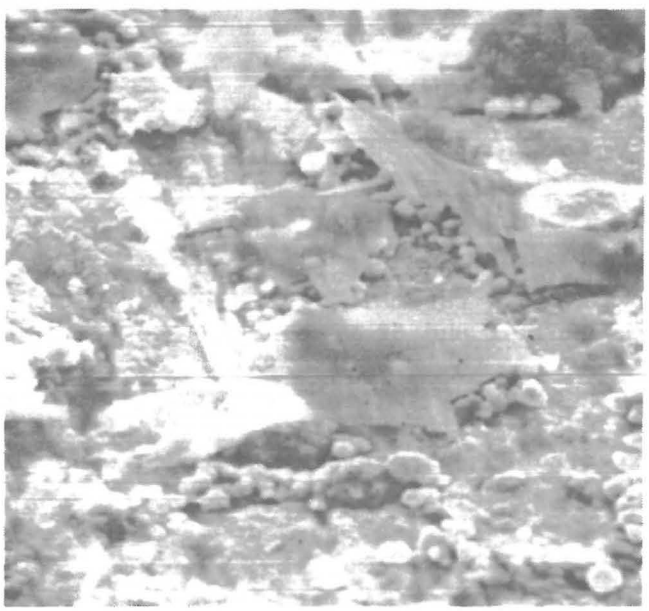

FIGURE 13.—Nodule formation after breakaway oxidation on alloy H at 900° C (X 2,000).

Alloy I was thermally cycled during 80 h of oxidation. Figure 17 shows the cross-sectional view and EDXA X-ray maps of alloy I. The internal oxidation and oxide penetration on this specimen are greater than those observed for alloy F but less than those for alloy G. This indicates that a higher Al content results in more internal oxidation and oxide penetration, whereas a higher Si content reduces both internal oxidation and oxide penetration. In most cases, little Fe was found in the oxide scale, and no concentration gradients of Si were observed in the metal phase.

The electron microprobe was employed to measure the concentration profile of Al, Cr, and Si. The accelerating voltage was 15 kV, and the scanning rate was 5 μm/min. The concentrations of Al and Cr in the metal both started to decrease about 25 to 30 μm from the scale-metal interface (fig. 18). Alloy F had more Cr depletion than did alloy G. Alloys G and I had a similar depletion of Al and Cr. High Al concentrations were observed when scanning through the internal oxidation regions. Silicon was not included in figure 18, since no concentration gradient was observed during scanning.

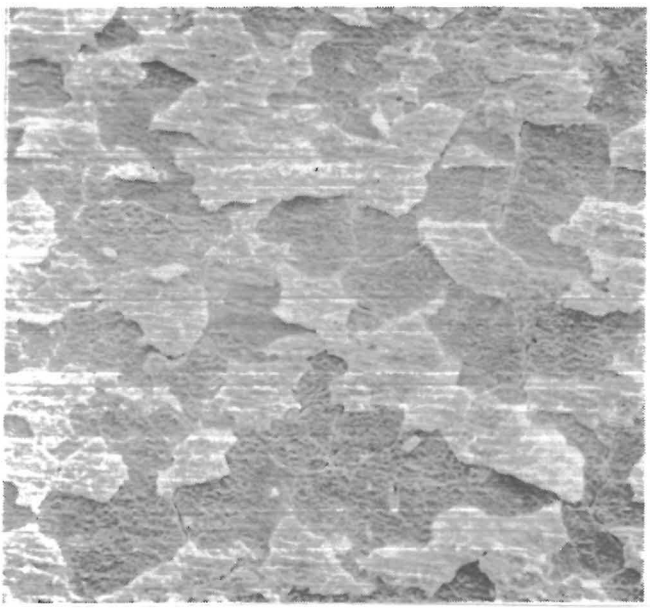

FIGURE 14.—Surface morphology of alloy D after 20 h of oxidation at 1,000° C (X 200).

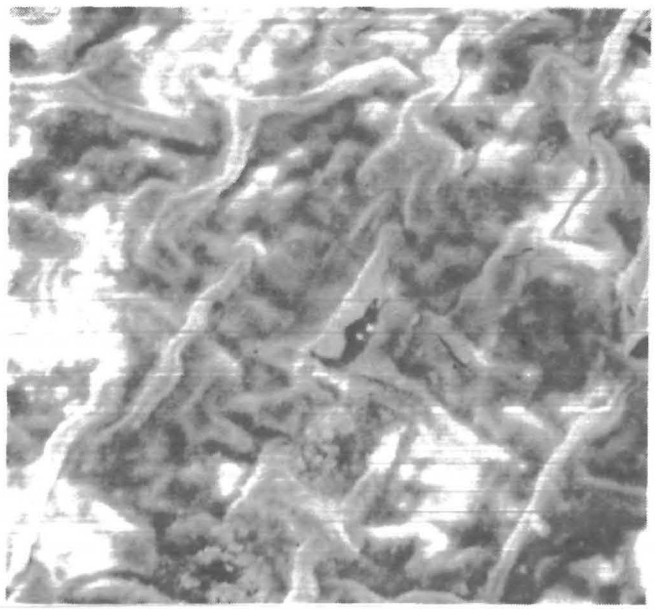

FIGURE 15.—Surface morphology of alloy G after 20 h of oxidation at 1,000° C (X 1,100).

DISCUSSION

The effect of alloying elements on high temperature oxidation was investigated, based on reaction kinetics and morphology of oxide and base metal.

The effect of Cr on oxidation resistance is well known. A protective Cr_2O_3 is formed on the metal surface during oxidation, resulting in a greatly reduced oxidation rate. However, a rapid oxidation rate is observed when the Cr content is low. Stephens and Barrett (1)[4] reported that an approximate lower limit for Cr for maintenance of acceptable oxidation and corrosion resistance was nominally 12 wt pct for modified 304 SS. Obviously, the 8 wt pct Cr used in the current study is not enough to form a continuous protective layer. However, small additions of Al and Si together with the Cr provide excellent oxidation resistance. This will be discussed in more detail later.

Thermodynamically, Ni forms the least stable oxide among the alloying elements in this study. As a result, it was not anticipated that Ni would provide any protection. Therefore, the major oxide observed by X-ray diffraction on the Fe-Ni binary alloy was Fe_2O_3, with a minor amount of Fe-Ni spinel. The same results were reported by previous investigators (2-4).

The ternary alloy C had better oxidation resistance than did binary alloys A and B. According to Hobby and Wood (5), Ni could more effectively dope Cr_2O_3 and/or absorb cation vacancies, producing a smaller vacancy activity gradient. This could be the reason for the lower oxidation rate in the ternary case.

When Al and Si were added to Fe-Cr-Ni ternary, the reaction kinetics and the morphology of the oxides were completely changed. Alloys D, F, G, H, and I exhibited better oxidation resistance than did 304 SS. These alloys had very small weight gains and formed extremely thin oxide layers, so it was impossible

[4]Underlined numbers in parentheses refer to items in the list of references at the end of this report.

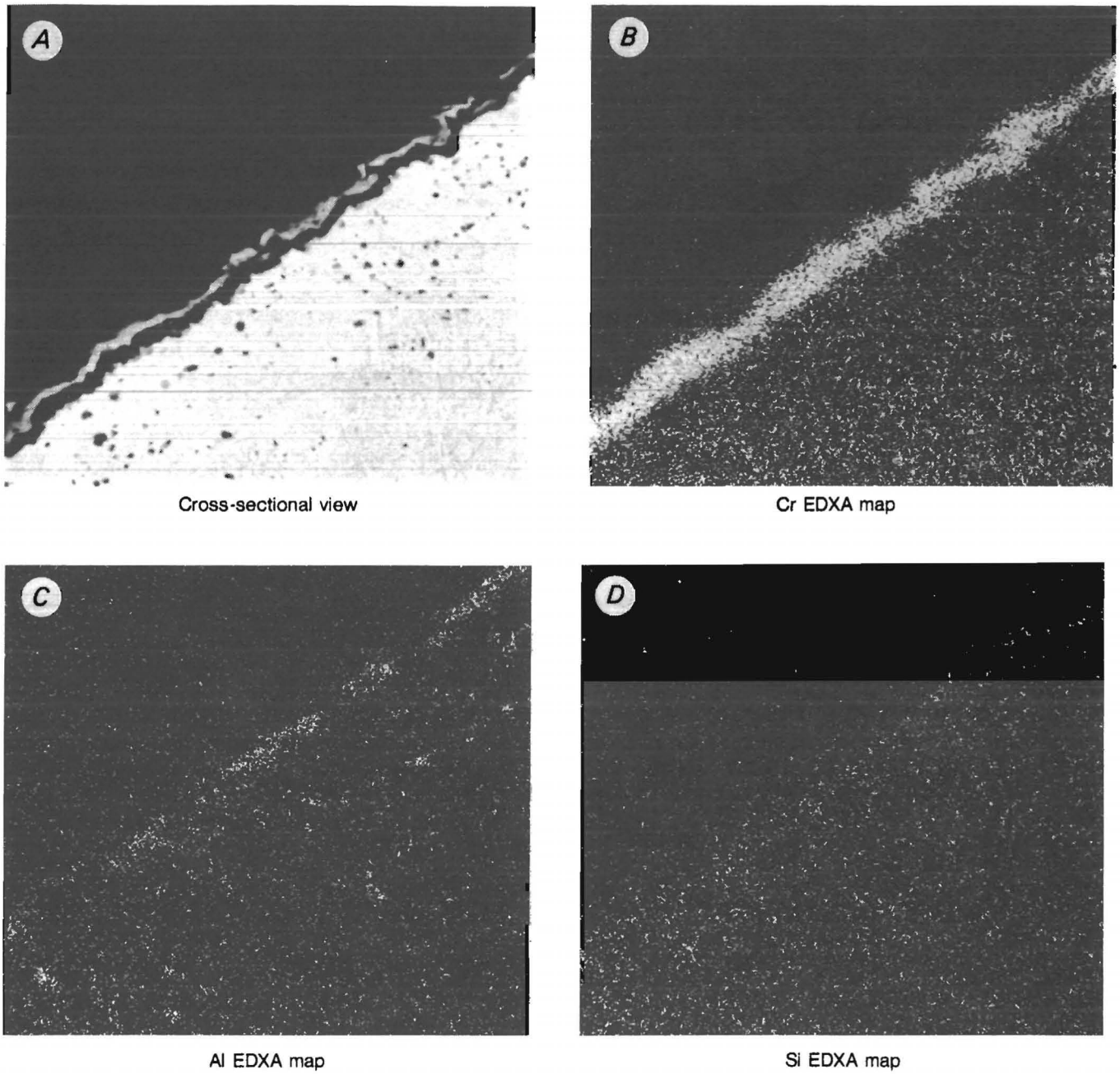

Cross-sectional view

Cr EDXA map

Al EDXA map

Si EDXA map

FIGURE 16.—Alloy F after several thermal cyclings for 40 h at 1,000° C (X 1,200).

to evaluate the effects of alloying elements and compositions of the oxide below 900° C. Note that the weight gains were only slightly greater than the accuracy of the balance; therefore, the reaction kinetics of alloys F, G, and I are essentially the same. More sophisticated instruments such as scanning-transmission electron microscopy, Auger electron microscopy, and/or electron energy loss spectroscopy are needed to analyze the compositions and profiles of the oxide layer.

At 900° C, these alloys, except alloy H, show better oxidation resistance than that of 304 SS. While this temperature is higher than that at which stainless steels are used in practice, the 900° C data gave more detailed information on the oxidation process and the effect of alloying elements. In the Fe-Al binary alloys, approximately 8 wt pct Al is

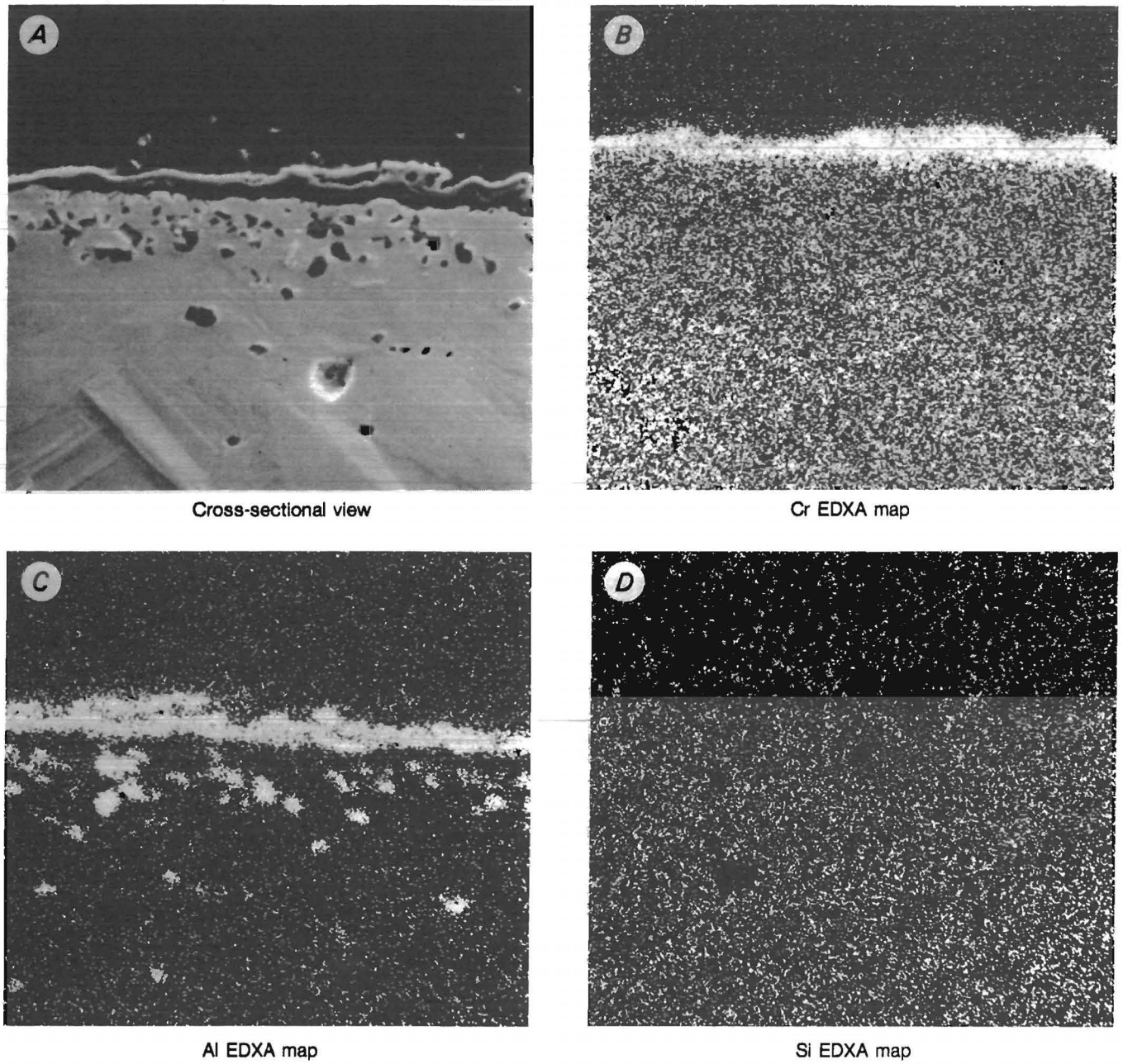

Cross-sectional view

Cr EDXA map

Al EDXA map

Si EDXA map

FIGURE 17.—Alloy I after several thermal cyclings for 80 h at 1,000° C (X 1,000).

sufficient to form an integral continuous external Al_2O_3 scale at 800° C; 5 wt pct Al is required at 1,000° C (6). Therefore, approximately 6 to 7 wt pct Al would be required to form a continuous Al_2O_3 scale at 900° C. Alloy H contained less than 3 wt pct Al; no protective layer was formed. However, the Cr acted as a secondary back-up element forming a protective layer. During thermal cycling of alloy H, breakaway oxidation was observed. Microcracks generally occur during thermal cycling. These cracks are usually due to different thermal expansion coefficients between metal and oxide. Penetration of gaseous O_2 through these cracks increases the oxygen potential at the scale-metal interface. Consequently, more oxidation can take place if there are not enough stable oxide-forming elements present in the alloy substrate. Both runs using alloy H

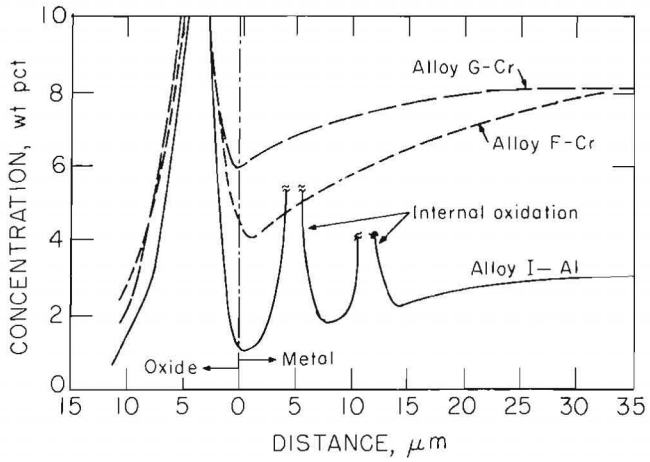

FIGURE 18.—Concentration profiles near metal-scale interface after 40 h of oxidation at 1,000° C.

produced similar results. Depletion of Al and Cr at the metal substrate led to breakaway oxidation.

When a small amount of Si was added, no breakaway oxidation was observed during thermal cycling. Alloy G, which was identical to alloy H but which contained 1.27 wt pct Si, had extremely small weight gains after thermal cycling. The effect of Si on high-temperature oxidation is well known (7-10). The Si forms silica or various silicates, depending on the Si content and temperature. When a Si-containing layer is formed, inward diffusion of oxygen and outward diffusion of metal cations are greatly suppressed. Alloy D, which contained only added Si, had good oxidation and thermal shock resistance. These results indicate that the addition of Si is better than that of Al when an equal amount of either element is added.

At 1,000° C, the individual effects of the alloying elements are more apparent. As shown in figures 14 and 15, the addition of Al combined with Si gives better oxide adherence. However, when Al additions exceed Si additions, internal oxides are found in the metal. Some of this oxide was observed deep in the metal. Alloy I exhibits less internal oxidation than does alloy G and less Cr depletion than alloy F. However, alloy I was the only alloy that exhibited poor hot-rolling workability in the form of edge cracks. Therefore, this alloy should not be considered as a 304 SS substitute. Although alloy F appears to be the best composition for a combination of oxidation, thermal shock resistance, and workability, it cannot be concluded that alloy F is the optimum choice because alloys D and G performed as well as alloy F below 1,000° C. Our main goal is to evaluate alloy substitutes for 304 SS at service temperatures less than 800° C. At this point, alloys D, F, and G perform better than does 304 SS. Our research demonstrates that the Cr content could be lowered to 8 wt pct if the synergistic effects of Al and Si additions are utilized.

It is obvious that the Si plays an important role in providing oxidation resistance. However, it is difficult to identify the extremely thin Si-containing layer using SEM and EDXA (11-13). Therefore, more sophisticated instruments and techniques are necessary to identify the layer. The continuation of this research is concentrating on the identification of a protective Si-containing layer so that a mechanism of oxidation can be proposed.

SUMMARY AND CONCLUSIONS

The oxidation characteristics of a series of Fe-Cr-Ni alloys with Si and Al additions are summarized in table 4 based on reaction kinetics and morphologies.

Several conclusions can be drawn regarding the effect of alloying elements:

1. Additions of both Al and Si greatly improve the oxidation and thermal shock resistance of low-Cr substitute alloys.

2. Aluminum gives better scale adherence that does Si. However, considerable internal oxidation was observed in the metal.

3. Silicon plays an important role in reducing both oxidation and internal oxidation.

4. Alloy F with additions of approximately 3.5 Si and 1.0 Al exhibited a favorable combination of properties.

TABLE 4. - Oxidation characteristics

Alloy	Characteristics	Oxide(s)
A, B, C, E.....	Highest oxidation with thick, columnar oxide.	Major Fe_2O_3 and minor spinel.
D.....	Good oxidation and thermal shock resistance; poor scale adherence.	Major Cr_2O_3 and minor spinel.
F.....	Good oxidation and thermal shock resistance; least internal oxidation and penetration.	Major Cr_2O_3 and minor Al_2O_3.
G.....	Good oxidation and thermal shock resistance; lots of internal oxidation and deepest oxide penetration.	Similar amounts of Al_2O_3 and Cr_2O_3.
H.....	Low oxidation.....	Major Al_2O_3.
	Breakaway oxidation.....	Major Fe_2O_3.
I.....	Good oxidation and thermal shock resistance and poor workability.	Similar amounts of Al_2O_3 and Cr_2O_3.

REFERENCES

1. Stephens, J., and C. Barrett. Substitution for Cr in 304 Stainless Steel. Ch. in Environmental Degradation of Engineering Materials. VPI, Blacksburg, VA, 1978, pp. 257-266.

2. Perrow, J. M., and W. W. Smeltzer. The Oxidation of an Iron-5 Per Cent Chromium Alloy in the Temperature Range 600°-850° C. J. Electrochem. Soc., v. 109, 1962, pp. 1023-1026.

3. Foley, R. T. Oxidation of Iron-Nickel Alloy. J. Electrochem. Soc., v. 109, 1962, pp. 1202-1206.

4. Menzies, I. A., and J. Lubkiewicz. Oxidation of an Fe-12%Ni Alloy in Oxygen at 700°-1,000° C. Oxid. Met., v. 3, 1971, pp. 41-58.

5. Hobby, M. G., and G. C. Wood. The Role of Nickel in the High-Temperature Oxidation of Fe-Cr-Ni Alloys in Oxygen. Oxid. Met., v. 1, 1969, pp. 23-42.

6. Sakiyama, M., P. Tomaszewica, and G. R. Wallwork. Oxidations of Iron-Nickel-Aluminum Alloys in Oxygen at 600°-800° C. Oxid. Met., v. 13, 1979, pp. 313-330.

7. Evans, J. W., and S. K. Chatter. Influence of Silicon on the High-Temperature Oxidation of Copper and Iron. J. Electrochem. Soc., v. 106, 1959, pp. 860-866.

8. Svedung, I., and N. G. Vannerberg. The Influence of Silicon on the Oxidation Properties of Iron. Corros. Sci., v. 14, 1974, pp. 391-400.

9. Kumar, A., and D. L. Douglass. Modification of the Oxidation Behavior of High-Purity Austenitic Fe-14Cr-14Ni by the Addition of Silicon. Oxid. Met., v. 10, 1976, pp. 1-22.

10. Evans, H. E., D. A. Hitton, R. A. Holm, and S. J. Webster. Influence of Silicon Additions on the Oxidation Resistance of a Stainless Steel. Oxid. Met., v. 19, 1983, pp. 1-18.

11. Yurek, G. J., D. Eisen, and A. Garnett-Reed. Oxidation Behavior of a Fine Grained Rapidly Solidified 18-8 Stainless Steel. Met. Trans. A, v. 13A, 1982, pp. 473-485.

12. Oh, J. M. Oxidation and Corrosion Properties of Austenitic Iron-Based Alloys Containing Manganese-Nickel-Silicon. Ph.D. Thesis, Univ. IL at Chicago, 1984, pp. 53.

13. Bennett, M. J., J. A. Desport, and P. A. Labun. Analytical Electron Microscopy of A Selective Oxide Scale Formed on 20%Cr-25%Ni-Nb Stainless Steel Oxid. Met., v. 22, 1984, pp. 291-306.

☆ U.S. GOVERNMENT PRINTING OFFICE: 1986—605-017/40,079

INT.-BU.OF MINES,PGH.,PA. 28349